

Integrated multi-omics analysis reveals common and distinct dysregulated pathways for genetic subtypes of Frontotemporal Dementia

Kevin Menden¹ (KM); Margherita Francescato¹ (MF); Tenzin Nyima¹ (TN); Cornelis Blauwendraat^{1,2} (CB); Ashutosh Dhingra¹ (Validation); Melissa Castillo Lizarido¹ (MC); Noémia Fernandes¹ (NF); Lalit Kaurani⁴ (LK); Deborah Kronenberg-Versteeg^{1,3} (DKV); Burcu Atarsu^{1,3} (BA); Eldem Sadikoglou¹ (ES); Barbara Borroni⁶ (BB); Salvador Rodriguez Nieto¹ (SRN); Javier Simon Sanchez^{1,3} (JSS); Andre Fischer⁴ (AF); David Wesley Craig⁷ (DWC); Manuela Neumann¹ (MN); Stefan Bonn^{1,5} (SB); Patrizia Rizzu¹ (PR); Peter Heutink¹ (PH).

Abstract

Understanding the molecular mechanisms underlying frontotemporal dementia (FTD) is essential for the development of successful therapies. Here, we present Phase 1 of a multi-omics, multi-model data resource for FTD research which will allow in-depth molecular research into these mechanisms. We have integrated and analysed data from the frontal lobe of FTD patients with mutations in MAPT, GRN and C9orf72 and detected common and distinct dysregulated cellular pathways. Our results highlight that excitatory neurons are the most vulnerable neuronal cell type and that vascular aberrations are a common hallmark in FTD. Via integration of multi-omics data, we detected several transcription factors and pathways which regulate the strong neuroinflammation observed in FTD-GRN. Finally, using small RNA-seq data and verification experiments in cellular models, we identified several up-regulated miRNAs that inhibit cellular trafficking pathways in FTD and lead to microglial activation. In this work we shed light on novel mechanistic and pathophysiological hallmarks of FTD. In addition, we believe that this comprehensive, multi-omics data resource will further mechanistic FTD research by the community.

Introduction

Frontotemporal Dementia (FTD) is a devastating pre-senile dementia characterized by progressive deterioration of the frontal and anterior temporal lobes¹. The most common symptoms include severe changes in social and personal behaviour as well as a general blunting of emotions. Clinically, genetically, and pathologically there is considerable overlap with other neurodegenerative diseases including Amyotrophic Lateral Sclerosis (ALS),

Progressive Supranuclear Palsy (PSP) and Cortical Basal Degeneration (CBD)². Research into FTD has made major advances over the past decades. Up to 40% of cases³ have a positive family history and up to 60% of familial cases can be explained by mutations in the genes Microtubule Associated Protein Tau (MAPT), Granulin (GRN) and C9orf72⁴ which has been key to the progress in our understanding of its molecular basis. Several other disease-causing genes have been identified that account for a much smaller fraction of cases⁵. Mutations in MAPT lead to accumulation of the Tau protein in neurofibrillary tangles in the brain of patients while mutations in GRN and C9orf72 lead to the accumulation of TDP-43⁶, as well as dipeptide repeat proteins (DPRs) and RNA foci in the case of C9orf72⁷.

As of today, no therapy exists that halts or slows the neurodegenerative process of FTD and in order to develop successful therapies there is an urgent need to determine whether a common target and therapy can be identified that can be exploited for all patients, or whether the distinct genetic, clinical and pathological subgroups need tailored treatments. Therefore, the development of remedies relies heavily on a better understanding of the molecular and cellular pathways that drive FTD pathogenesis in all FTD subtypes.

Although our knowledge of FTD pathogenesis using molecular and cellular biology approaches has significantly advanced during recent years, a deep mechanistic understanding of the pathological pathways requires simultaneous profiling of multiple regulatory mechanisms. As neurodegenerative diseases develop over time, it is furthermore important to examine temporal changes. While post-mortem human brain tissue is not suitable for this aspect, well-defined rodent models can be used to address the temporal component. Lastly, experimental validation of derived hypotheses can be achieved in cellular systems, such as neurons derived from induced pluripotent stem cells (iPSCs) as well as in rodent models. To address these issues, the Risk and modifying factors in Frontotemporal Dementia (RiMod-FTD) consortium⁸ generates a multi-model and multi-omics data resource with the focus on mutations in the three most common causal genes: MAPT, GRN and C9orf72. The data resource will consist of multi-omics datasets from multiple post-mortem human brain regions, and matching iPSC derived neurons and brain tissue of transgenic mouse models at different time points.

Here, we report on the data of Phase 1 in which we have extensively analysed and integrated post-mortem human brain RNA-seq, CAGE-seq, smRNA-seq and methylation datasets from RiMod-FTD. We identified dysregulation of overlapping pathways in all disease groups that indicates converging disease mechanisms manifesting during disease progression. Using deconvolution analysis, we have identified changes in cellular composition that are either common or distinct to genetic subgroups. Through integration of smRNA-seq and CAGE-seq data, we could furthermore highlight potential regulatory molecules that might play important roles in FTD pathogenesis, within the identified functional gene modules and pathways. The RiMod-FTD data will be freely accessible to the scientific community through the European Genome-phenome Archive (EGA) and a dedicated RiMod-FTD web application thus enabling scientists to derive new mechanisms and hypotheses from the data.

Results

Multi-omics Data Resource for Frontotemporal Dementia

In an ongoing effort we have analysed data from brain tissue from diseased patients carrying mutations in the MAPT (n=17), GRN (n=11) or C9orf72 (n=17) genes and non-demented controls (n=16). As expected, the average age of FTD groups was lower than that of healthy controls (Table S1). We obtained tissue from up to 7 regions for each brain. The temporal and frontal lobes are the most affected areas in FTD, but we also obtained material from the occipital lobe, hippocampus, caudate, putamen and cerebellum for verification experiments. We performed CAGE-seq, smRNA-seq and quantitative proteomics (Miedema et al., manuscript in preparation) on tissue from frontal and temporal lobes, and additionally generated methylation and RNA-seq data for frontal lobe tissue. Additional data types such as ATAC-seq are planned for future releases. The resulting, comprehensive multi-omics data resource enables the study of disease mechanisms in FTD subtypes to greater detail than single genomics experiments (Fig. 1).

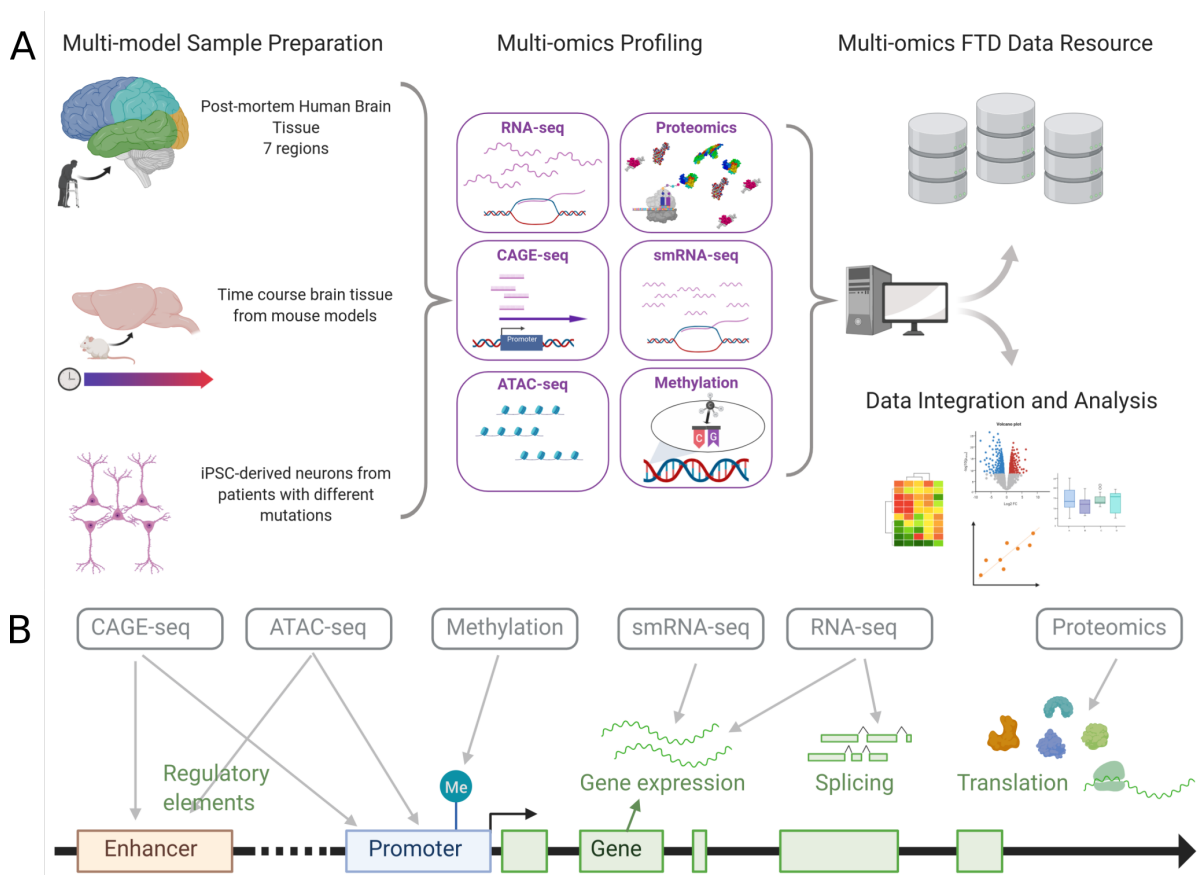


Figure 1: Graphical overview of the RiMod-FTD project. A In phase 1, Human Post-mortem brain tissue samples from multiple regions of patients with mutations in GRN, MAPT and C9orf72 have been collected and used for multi-omics data generation. The datasets have been integrated and analysed and published to be accessible as FTD resource. In subsequent phases additional datatypes will be added (i.e. ATACseq) and the resource will be extended with data from matching mouse models and iPSC derived celltypes. **B** The multi-omics approach allows to profile multiple regulatory features of gene expression,

including enhancer- and promoter-based regulation, epigenetic regulation, alternative splicing, post-transcriptional regulation (miRNAs) and regulation of translation (proteomics).

In this study, we have integrated RNA-seq, CAGE-seq, smRNA-seq and methylation data from the Gyrus Frontalis Medialis (GFM) (Table S2), as this brain region is strongly affected in FTD. To validate observed transcriptomics dysregulation effects, we performed miRNA inhibition and mimic experiments in iPSC-derived neurons and microglia.

Differential gene expression analysis and cellular deconvolution of the GFM in FTD

To identify general gene expression patterns in the GFM of patients with FTD, we performed differential gene expression (DGE) and principal component analysis (PCA) using the RNA-seq data. The PCA indicates considerable heterogeneity between samples, as can be expected from post-mortem human brain tissue (Fig. 2A). However, a difference between FTD cases and control samples is clearly visible. Differentially expressed genes (DEGs) were calculated for all disease groups (FTD-MAPT, FTD-GRN, FTD-C9orf72) compared to controls while controlling for gender and pH-value (see Methods). We observed the largest number of DEGs (adj. P-value < 0.05) for FTD-GRN, followed by FTD-MAPT and FTD-C9orf72 (Fig. 2B). DGE of smRNA-seq data yielded 78, 21 and 39 differentially expressed miRNAs in FTD-MAPT, FTD-GRN and FTD-C9orf72, respectively (Fig. 2C). As we detected relatively few DEGs for FTD-C9orf72, some analyses could only be performed for FTD-MAPT and FTD-GRN.

Due to the neurodegenerative nature of FTD, it is likely that there exists a systematic difference in cell composition between cases and controls which can affect DGE analysis due to differences in gene expression between cell types - a problem which has often been overlooked in tissue expression studies. Here, we tried to account for this problem by applying a conservative filtering approach and removing DEGs that are associated with changing cellular composition (see Methods). All further analyses were based on the filtered set of DEGs, unless otherwise specified. Note that this method could only be applied to the total RNA-seq dataset because similar cell type specificity data (here, single-cell RNA-seq data) was not available for other data types.

Activation of extracellular matrix (ECM) associated pathways and circulatory system development.

We next performed pathway enrichment analysis with DEGs from the RNA-seq data using go:Profiler⁹ to identify the most affected cellular pathways. Down-regulated genes are strongly enriched for mitochondrial and oxidative phosphorylation pathways in both FTD-GRN and FTD-MAPT (Fig. 2D, Fig. S1), indicating a dysfunctional energy metabolism - a well-known hallmark of many neurodegenerative diseases¹⁰. Neuronal system pathways are enriched among down-regulated genes for both groups as well. This might be explained by dysfunctional neurons that have not yet undergone apoptosis or by a general impairment of neuronal function caused by the disease. Other significantly down-regulated pathways include ubiquitin-dependent protein metabolism and vesicle-mediated transport (FTD-GRN).

In all three groups, up-regulated genes are enriched for extracellular matrix (ECM) associated pathways and circulatory system development (Fig. S1). Genes involved in Hippo-signalling are enriched in FTD-GRN and FTD-MAPT (Fig. 2D), and immune system related genes are enriched in FTD-GRN. ECM dysregulation, in particular, has been implicated with several neurodegenerative diseases. For instance, studies in mouse models showed that tau pathology can lead to ECM reorganization and that reducing ECM proteins could reverse memory deficits in an AD model^{11,12}. While the role of the ECM in FTD remains unknown, our results suggest a prominent involvement in end-stage FTD.

We also specifically examined the DEGs with the largest fold-changes in the RNA-seq data because large expression fold-changes often signify strong dysregulation. These results support the importance of ECM in FTD as for all disease groups, multiple matrix metalloproteinase enzymes (MMPs) are among the DEGs with the largest LFCs (Fig. S2, Fig. S3A). Elevated RNA levels of MMP genes have been reported for many neurodegenerative diseases, and MMPs target a wide range of ECM¹³ indicating their importance in neurodegenerative mechanisms¹⁴. Protein interaction networks of up-regulated genes in FTD-MAPT and FTD-GRN show the central importance of MMPs in these networks (Fig. S3 B & C).

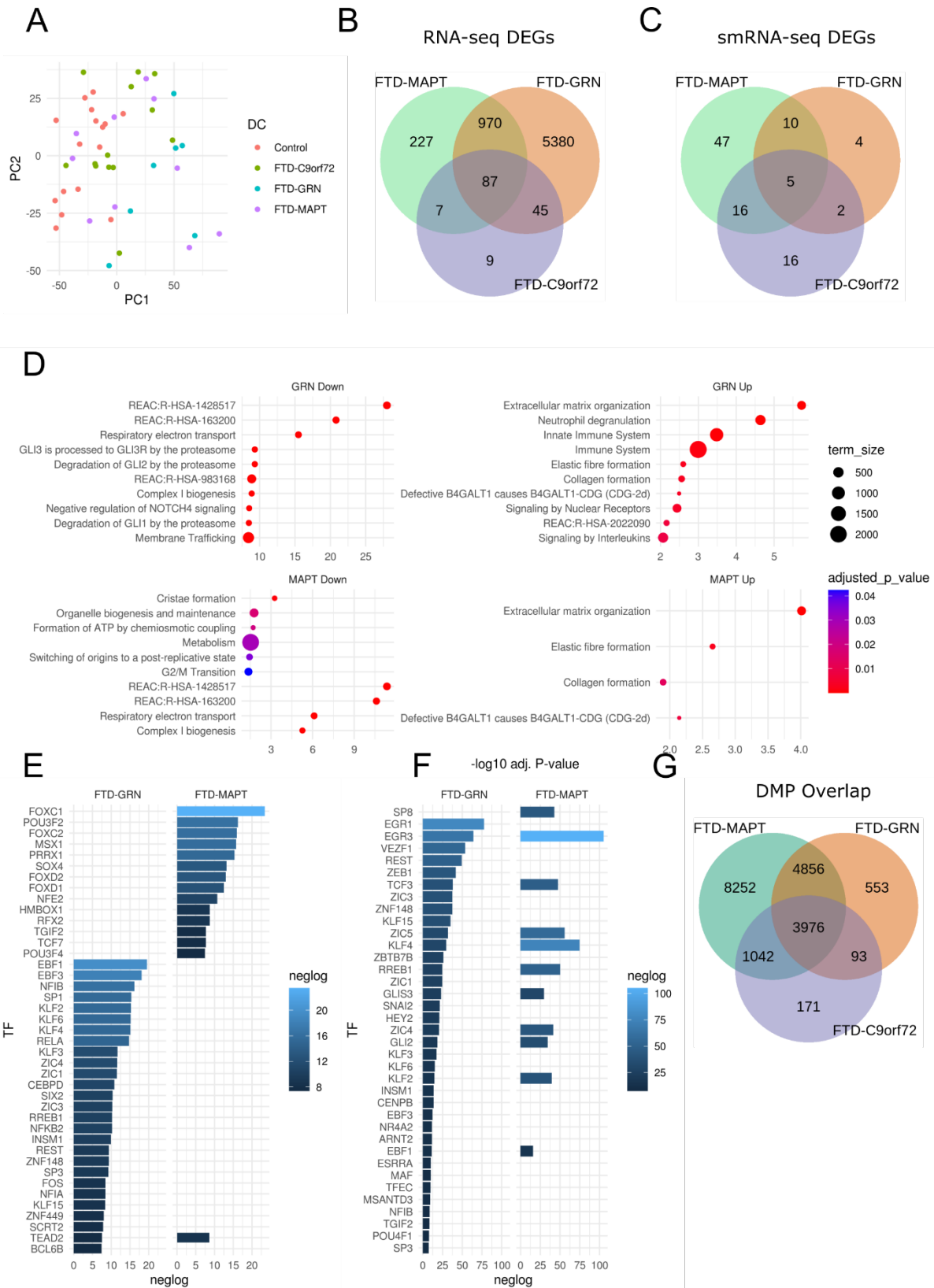


Figure 2: Gene- and Pathway-level transcriptional changes in FTD. A Principal component analysis of variance stabilized RNA-seq expression values, coloured by group. **B** Overlap between RNA-seq DEGs from different disease groups. **C** Overlap between smRNA-seq DEGs from different disease groups. **D** Enriched Reactome pathways in RNA-seq up- and down-regulated DEGs. Shown are the ten most significant pathways per group;

the x-axis signifies the negative log₁₀ P-value. Colour corresponds to adjusted P-value and node size corresponds to the number of genes in a pathway. **E, F** Best candidates for active and inactive TFs in FTD-GRN and FTD-MAPT, respectively. The x-axis signifies the negative log₁₀ P-value. **G** Overlap of DMPs in different disease groups.

Regulatory mechanisms associated with differential expression

To better understand relevant regulatory mechanisms leading to these gene expression changes, we generated a set of candidate driver transcription factors (TFs) using the GFM CAGE-seq data. CAGE-seq cluster counts, when assigned to the closest gene, correlate well with RNA-seq expression data (average sample-wise correlation coefficient: 0.6, Fig. S4). We used the CAGE-seq data to predict candidate driver TFs for up- and down-regulated genes (see Methods for details). TEAD2, a TF central to the Hippo signalling pathway, is the only predicted active TF common to FTD-GRN and FTD-MAPT (Fig. 2E), while there is greater overlap among inactive TFs (here: inactive TF = has down-regulated targets, Fig. 2F). Moreover, we performed miRNA-target gene mapping to evaluate potential regulatory roles of miRNAs. Expression values of miRNAs were correlated with their predicted targets using matching samples from the RNA-seq data. Only miRNA-target pairs with considerable negative correlation were retained (see Methods).

DNA methylation is another important regulatory mechanism that can affect gene expression. We used the Illumina Infinium EPIC methylation data from the GFM to examine epigenetic changes in FTD. We considered only the most variable CpG sites (28,173) and corrected for possible confounding effects using surrogate variable analysis (SVA) to perform differential methylation analysis (see Methods). We detected 18,126, 9,478 and 5,282 significantly differentially methylated positions (DMPs) for FTD-MAPT, FTD-GRN, and FTD-C9orf72, respectively (Fig. 2G). The C9orf72 repeat expansion is known to be associated with hypermethylation¹⁵ and we confirmed in our data that a CpG site located at the 5'-end of the C9orf72 gene, only 14 bp away from the repeat expansion, is hypermethylated (log fold-change: 0.6, Fig. S4A). Pathway enrichment analysis of genes in proximity to DMPs yielded enrichment of genes involved in nervous system development for hypermethylated CpG sites. Genes close to hypomethylated sites were enriched for system development and vasculature development (Fig. S5C). As hypermethylation of CpG sites at promoter regions is associated with decreased expression, this indicates epigenetically controlled expression inhibition of genes important for neuronal function, or remnants of cell composition effects that could not be entirely alleviated by SVA (see Methods). Performing biological age prediction using the methylation data resulted in underestimated age predictions for all groups, albeit to a lesser extent for FTD groups, which indicates accelerated aging in FTD (Fig. S5B).

Vulnerability of excitatory neurons and enrichment of endothelial cells

To identify vulnerable cell types and disease-related cell composition changes, we inspected the results from the RNA-seq deconvolution analysis (Methods) with respect to genetic FTD subtypes. As expected, fractions of neuronal cells are systematically lower in all FTD groups compared to controls (Fig. S6). As a result, virtually all other cell types show increasing percentages. We therefore calculated the percentage-wise change for each cell type and assessed statistical significance (see Methods). Strongest neuronal loss was observed in FTD-GRN, followed by FTD-MAPT and FTD-C9orf72 (Fig. 3A, Table S3), which agrees with studies that have shown that the frontal lobe is most strongly affected in FTD-GRN^{16–18}. Moreover, neuronal loss can be primarily attributed to loss of excitatory neurons, while fractions of inhibitory are not significantly different to controls (Table S3). Our results therefore confirm findings from recent studies that found excitatory neurons to be especially vulnerable to tau pathology¹⁹ and detected an important role of glutamatergic neurotransmission in FTD^{20,21}. Closer examination of the KEGG pathway ‘glutamatergic synapse’ suggests that AMPA receptors are mainly affected, while we could not see signs of dysregulation for NMDA receptors (Fig. S7 A-C). Analysis of candidate regulator TFs highlighted the TF Early Growth Response 3 (EGR3), targets of which are enriched for glutamatergic synapse genes (Fig. S7D), indicating involvement in excitatory neuronal function.

To validate the results of our computational deconvolution, we considered the fractions of excitatory neurons as a proxy of neurodegeneration and correlated them with manually determined degeneration scores from a pathologist (Fig. 3B, Methods). Indeed, excitatory neuron fractions show strong negative correlation with pathology scores (Pearson’s correlation coefficient = -0.78, P-value = 2.8e-07), thereby providing experimental confirmation of our computational predictions.

The strongest growth in percentage compared to the baseline is observed for endothelial cells in FTD-MAPT and FTD-C9orf72 disease groups, but not FTD-GRN, where microglial cells show the strongest increase. Circulatory system development is among the most significantly up-regulated biological processes in all three disease groups (Fig. 3 C & D). The role of the circulatory system in FTD is relatively unexplored, however, Bennet et al. recently found increased vasculature growth in mouse models of FTD-MAPT with P301L mutation²². Interestingly, endothelial enrichment in FTD-MAPT is particularly strong in patients with P301L mutation (Fig. 3A). Another recent study observed a particular microvascular structure with increased frequency in brains of patients with frontotemporal lobar degeneration (FTLD)²³ and Park et al. have shown that soluble tau can interfere with nitric oxide production and thus lead to reduced vasodilation of blood vessels, ultimately leading to insufficient blood supply²⁴.

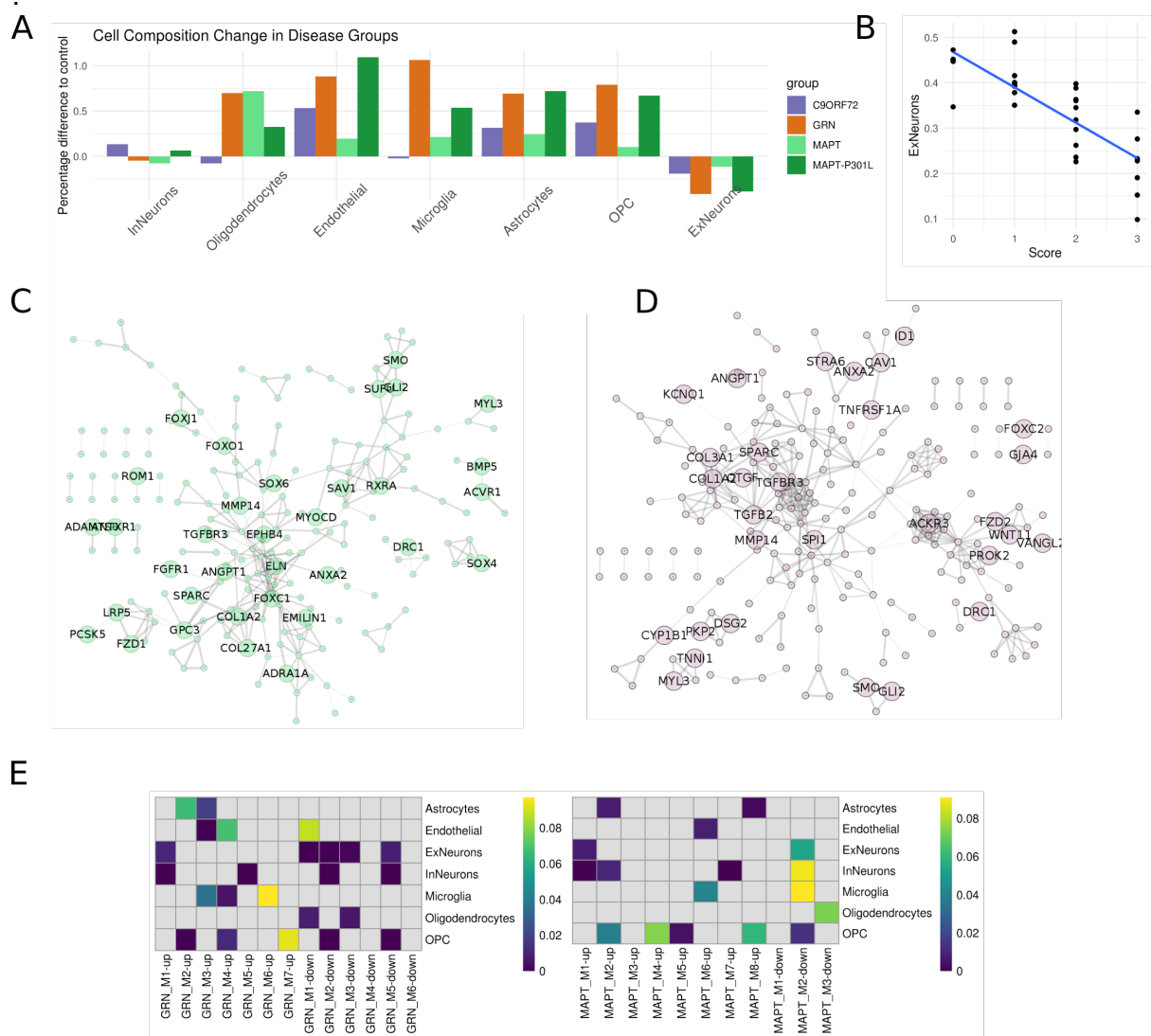


Figure 3: Cell composition changes in FTD. A Percentage change of averaged fractions per group compared to the average of the control group. Genetic subtypes are indicated with different colours. **B** Regression of excitatory neuron fractions (y-axis) against neuropathology scores (x-axis). **C, D** PPI networks of genes up-regulated in FTD-MAPT and FTD-GRN (log-fold-change > 1), respectively. Genes involved in the biological process “circulatory system development” are labelled. **E** Heatmap of EWCE analysis results for HumanBase modules of FTD-GRN and FTD-MAPT. Different modules are lined up on the x-axis, different cell types on the y-axis. Tile colour signifies the EWCE P-value. Tiles with P-values above 0.1 are marked grey.

To better understand transcriptional changes and regulatory mechanisms, it is often helpful to cluster genes into modules with similar expression or function. Therefore, we performed tissue-specific functional module detection with HumanBase²⁵ and assessed cell type specificity of modules using EWCE²⁶. Both for FTD-MAPT and FTD-GRN, most modules show specificity for a few cell types (Fig. 3E). Up-regulated modules in both groups are significantly enriched for endothelial genes (P-value < 0.1). Genes within these modules have been associated with blood vessel development (FTD-MAPT M6-up) and endothelial

cell growth (FTD-GRN M4-up) by HumanBase (Fig. 3 C & D), further supporting a distinct involvement of endothelial genes in these FTD subtypes.

Increased Inflammatory response in FTD-GRN

The protein encoded by GRN is well known for its importance to lysosomal function and as a modulator of the immune system, among others²⁷. Finally, in patients with FTD-GRN, microglial fractions show an even larger relative increase than endothelial cells, indicating increased microglial activity. GRN is highly expressed in microglia and well-known for having important functions in the immune system²⁸. Microglia are also slightly enriched in FTD-MAPT (P-value = 0.037) but not in FTD-C9orf72 (P-value = 0.475).

Here, we have observed a prominent increase in microglial cell fractions and up-regulation of immune system pathways in FTD-GRN, a feature of GRN deficiency that has been frequently shown in mouse models²⁸⁻³⁰. We therefore wanted to further characterize potential underlying regulatory mechanisms. First, we examined FTD-GRN modules for enrichment of immune system-related terms. Indeed, several up-regulated modules are enriched for genes related to the immune system, while we could not find enrichment among down-regulated modules. The module FTD-GRN M1-up contains genes important for neutrophil migration and response to interleukins (Fig. 4 A & D). Both modules M3-up and M4-up contain genes relevant to NF-kappa-B (NFkB) signalling, as well as genes involved in tumour necrosis factor (TNF) production (Fig. 4 B & C, respectively). Finally, the module M6-up is enriched for genes involved in T cell activation. Modules M3-up, M4-up and M6-up are furthermore enriched for microglial-specific genes (Fig. 3E). Interestingly, several necroptosis-related genes are up-regulated (M1-up: TLR3, TLR8, RIPK3; M4-up: RIPK2), suggesting this pathway as a potential driver of neuronal death. While we did not detect prominent signals for neuroinflammation in FTD-MAPT, the FTD-MAPT module M3-up contains several genes involved in T cell and TNF signalling (EZR, RAB29, CARD8, HIPK1). However, neuroinflammation is much less prominent in FTD-MAPT and FTD-C9orf72 compared to FTD-GRN.

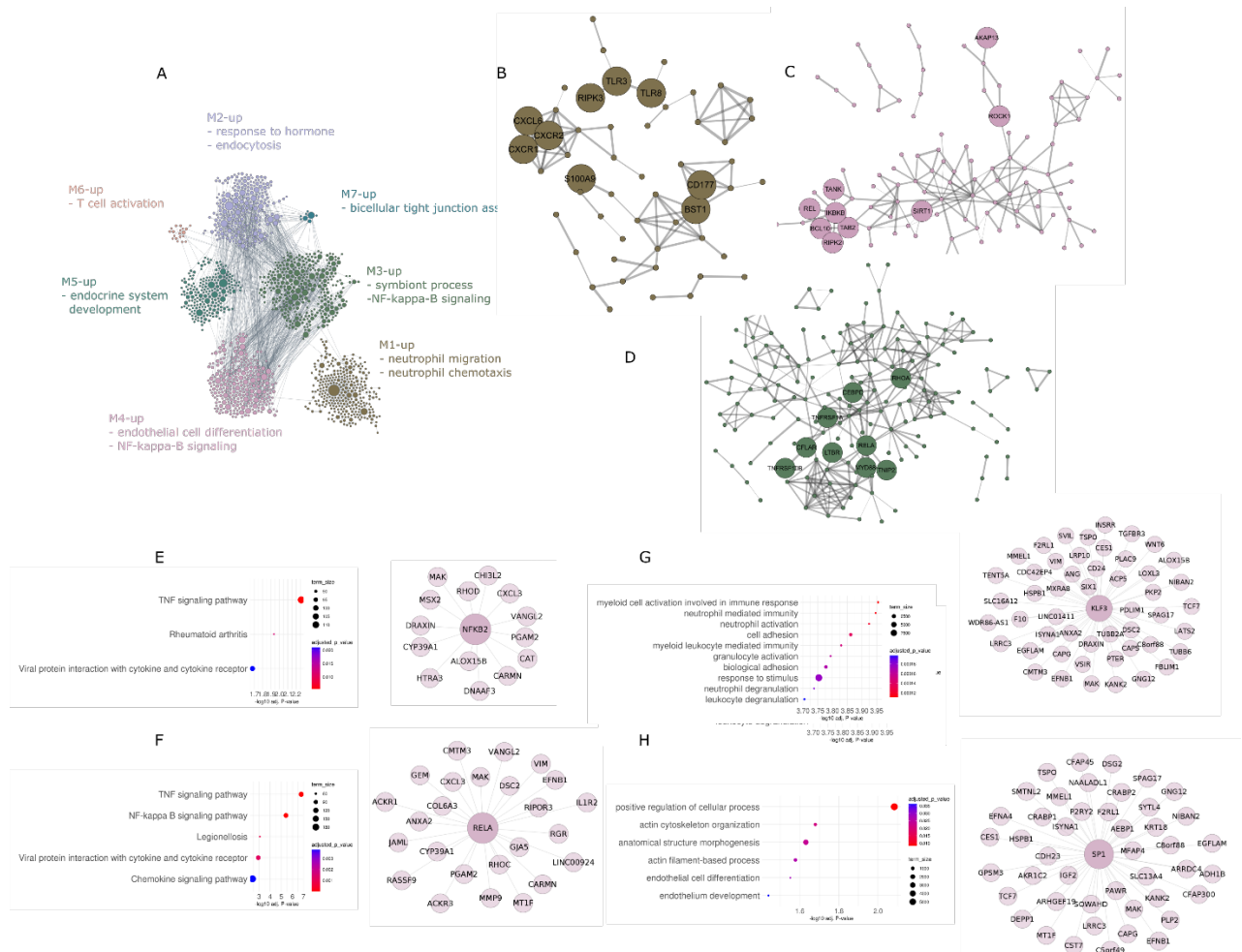


Figure 4: Neuroinflammation in FTD-GRN. **A** Up-regulated HumanBase modules in FTD-GRN with most significant terms. **B** Protein-protein interaction (PPI) network (made with String-DB) of FTD-GRN M1 up-module. Genes involved in necroptosis, interleukin response and neutrophil migration are indicated **C** PPI network of FTD-GRN M4-up module. Genes involved in NFkB signalling are indicated. **D** PPI network of FTD-GRN M3-up module. Genes involved in NFkB signalling and CEPBD are indicated. **E** and **F** KEGG pathway enrichment of predicted targets of TFs NFKB2 and RELA, respectively. **G** and **H** GO:BP pathway enrichment of predicted targets of TFs KLF3 and SP1, respectively.

Inspection of our candidate regulator TFs indicated the TFs Nuclear Factor Kappa B Subunit 2 (NFKB2) and RELA as potential drivers in FTD-GRN (Fig. 2E), which together form the NFkB signalling complex. Enrichment analysis of predicted NFKB2 and RELA targets in FTD-GRN revealed TNF signalling and NFkB signalling as the most significantly enriched KEGG pathways (Fig. 4 E & F), suggesting NFKB2 and RELA as potential drivers of increased TNF signalling. Furthermore, enrichment analysis indicated targets of the TFs SP1 and KLF3 as highly enriched among genes in the FTD-GRN M3-up module, which are both part of our candidate regulator set. Predicted KLF3 targets are enriched for immune system genes (Fig. 4G). SP1 target genes do not show a strong enrichment but have roles in actin cytoskeleton organization and endothelial cell differentiation, among others (Fig. 4H). We furthermore investigated predicted targets of down-regulated miRNAs and genes proximal to

hypomethylated CpG sites for involvement in the immune system in FTD-GRN but could not detect any significant immune system-relevant enrichment.

To closer examine which parts of the NFkB and TNF signalling pathways are affected in FTD-GRN and in FTD in general, we inspected fold-changes of genes from the corresponding KEGG pathways. Interestingly, the pro-inflammatory cytokine Interleukin 1 Beta (IL1B) is down-regulated in all disease groups, although only significantly in FTD-MAPT (Fig. S9A). Similarly, the inflammatory cytokine Interleukin 6 (IL6) has negative fold-changes in all disease groups. Downstream effector genes with positive fold-changes include multiple chemokines, Interleukin 18 Receptor 1 (IL18R1) and several metalloproteinases.

Hyperactivation of TNF by NFkB signalling has been linked to obsessive-compulsive behaviour in a GRN loss-of-function mouse model²⁹. The authors found that GRN deficiency leads to NFkB overactivation in microglia, and that inhibition of NFkB was sufficient to rescue the behavioural symptoms. Indeed, it has been previously shown in mice that GRN deficiency leads to overactivation of microglia²⁸.

Dysfunctional energy metabolism and cellular trafficking in FTD

Among the most significantly down-regulated pathways in FTD-GRN and FTD-MAPT are several pathways involved in energy metabolism and oxidative phosphorylation (Fig. 2D, Fig. S1). Inspection of modules revealed the modules FTD-GRN M1-down and FTD-MAPT M1-down as being most significantly associated with the term NADH dehydrogenase complex assembly (Fig. 5 D & E, Tables S4 and S5). Further inspection of the FTD-MAPT and FTD-GRN M1-up modules revealed that they contain several NADH:Ubiquinone Oxidoreductase Subunit genes (Fig. 5 B & C), which are necessary for functional oxidative phosphorylation and hence energy production. The FTD-GRN module is moreover enriched for genes involved in intracellular transport and autophagy. The FTD-GRN M1-down module contains several genes associated with FTD or ALS: Superoxide Dismutase 1 (SOD1), Dynactin Subunit 1 (DCTN1), PTEN Induced Kinase 1 (PINK1), Huntingtin (HTT), and CHCHD10. All these genes show lower expression values in every genetic subgroup, although they do not reach significant levels in all groups (Fig. 5A).

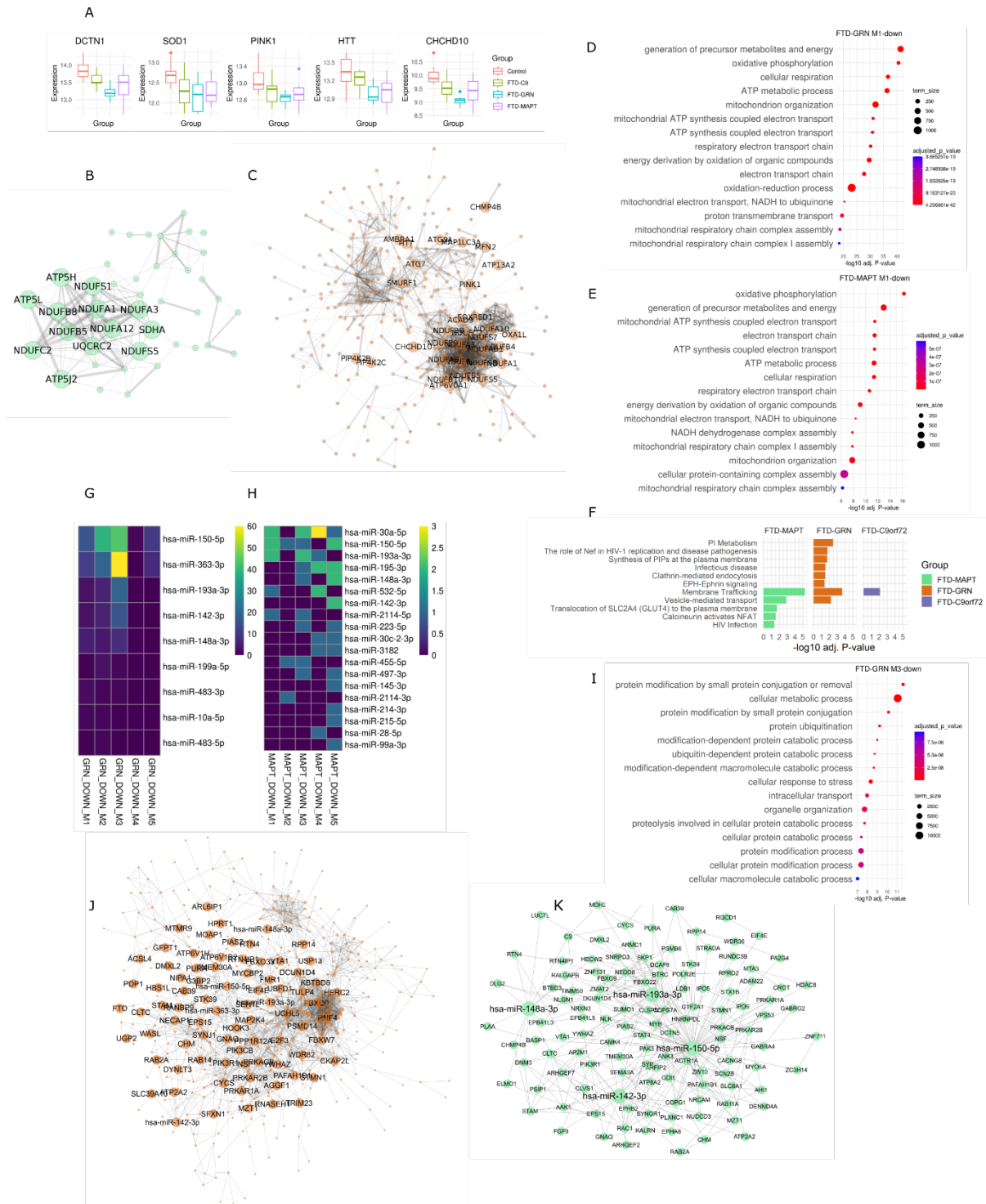


Figure 5: Impaired oxidative phosphorylation and cellular trafficking in FTD. A Expression levels (variance stabilized with DESeq2) of the genes CHCHD10, PINK1, SOD1, DCTN1 and HTT in different groups. **B** STRING-DB PPI of FTD-MAPT M1-down module. Genes involved in oxidative phosphorylation are labelled. **C** PPI of FTD-GRN M1-down module. Genes involved in NADH dehydrogenase complex assembly and mitophagy are labelled, as well as CHCHD10. **D, E** Most significant results from pathway enrichment analysis with g:Profiler (GO biological process) for the FTD-GRN M1-down module and the FTD-MAPT M1-down module, respectively. Node colour corresponds to adjusted P-value and node size to term size. **F** Most significant results from enrichment analysis (Reactome)

of targets of up-regulated miRNAs in all disease groups. **G, H** Heatmaps of intersection-over-union scores between predicted miRNA targets and down-regulated modules in FTD-GRN and FTD-MAPT, respectively. **I** Top enrichment results of g:Profiler (GO biological process) for the FTD-GRN M3-down module. Node colour corresponds to adjusted P-value and node size to term size. **J** PPI network (String-DB) of FTD-GRN M3-down module. Predicted targets of up-regulated miRNAs are labelled. **K** PPI network of predicted targets of up-regulated miRNAs in FTD-MAPT.

Cellular transport is thought to play a key role in FTD pathogenesis as impaired trafficking can affect protein and mitochondria homeostasis. Here, we have shown that mitochondria function is strongly impaired in end-stage FTD and that transport pathways are tightly connected to this pathology. We thus looked for potential regulatory mechanisms driving the pathological changes. Enrichment analysis of targets of up-regulated miRNAs in all disease groups revealed cellular localization as the most significantly enriched biological process (GO:BP) and membrane trafficking as the most significant Reactome pathway (Fig. 5F). Up-regulated miRNAs in FTD therefore seem to primarily target cellular transport pathways and might play important roles in dysfunctional transportation.

To detect modules and genes predominantly targeted by up-regulated miRNAs, we calculated the intersection-over-union (IoU) of up-regulated miRNA targets with down-regulated modules for FTD-GRN and FTD-MAPT (Fig. 5 G & H). The FTD-GRN M3-down module is most strongly targeted by miRNAs and contains genes involved in metabolic processes and cellular localization (Fig. 5I, Table S4). Five miRNAs have putative target genes in this module: hsa-miR-150-5p, hsa-miR-142-3p, hsa-miR-193a-3p, hsa-miR-148a-3p and hsa-miR-363-3p, which are all significantly up-regulated in FTD-MAPT as well, except hsa-miR-363-3p. We generated networks of the above mentioned candidate miRNAs combined with a PPI network of the FTD-GRN M3-down module (Fig. 5J) and a PPI network of all predicted targets in FTD-MAPT (Fig. 5K), as we could not detect a similar module in FTD-MAPT. In total, we observed 31 common putative miRNA targets in both networks.

Next, we selected three miRNAs for further characterization in our cellular model systems: hsa-miR-193a-3p, hsa-miR-150-5p and hsa-miR-19b-3p (Fig. 6A). The former two miRNAs are DE in all three disease groups and have many targets among module genes (Fig. 5 J & K). The miRNA hsa-miR-19b-3p is up-regulated in all disease groups, although it does not reach significance after (FTD-MAPT and FTD-C9orf72) or before (FTD-GRN) multiple testing correction. Nevertheless, down-regulated genes were predicted to be enriched for targets of hsa-miR-19b-3p by g:Profiler, the miRNA is known to inhibit autophagy³¹ and it is highly expressed in neurons. We performed RNA-seq experiments on iPSC-derived neurons and microglia (Methods) that were transfected with miRNA mimics and inhibitors for the three selected miRNAs. Here, we focused on the mimic experiments, as the mimics should in theory reproduce the effects of miRNA overexpression. Inhibition and mimicking of miR-150-5p in neurons had only minor effects in neurons, while in microglia, the miR-150-5p mimic had strong effects, leading to 237 down-regulated and 236 up-regulated DEGs, enriched for cellular transport and immune system pathways of the latter and nervous system development of the former (Fig. 6B). Inhibition of miR-150-5p had even stronger effects (3221 DEGs), indicating an important function of this miRNA in microglia. Transfection of miR-193a-3p mimic and inhibitor was only successful in microglia, where the mimic had strong effects with 1756 down-regulated and 1474 up-regulated genes. Up-regulated genes

were enriched of mitochondrial functions like oxidative phosphorylation, while down-regulated genes were enriched for localization and vesicle-mediated transport pathways (Fig. 6C).

In neurons, the miR-19b-3p mimic resulted in 89 down- and 137 up-regulated DEGs (inhibitor: 8 down-regulated, 31 up-regulated). Genes down-regulated by the mimic and up-regulated in the inhibitor experiment are involved in neuronal system pathways, enriched for miR-19b-3p targets and share 17 common genes, thus providing evidence for these genes to be regulated by miR-19b-3p. In microglia, stronger effects of the miR-19b-3p mimic compared to the inhibitor were observed (1518 compared to 608 DEGs). Genes down-regulated by the miR-19b-3p mimic were enriched for catabolic processes, autophagy and vesicle-mediated transport, up-regulated genes were enriched for cell cycle and immune system related genes (Fig. 6D). These results provide strong evidence that hsa-miR-19b-3p and hsa-miR-193a-3p indeed regulate cellular trafficking pathways. Furthermore, hsa-miR-150-5p is important for microglia function and up-regulation could lead to immune system activation.

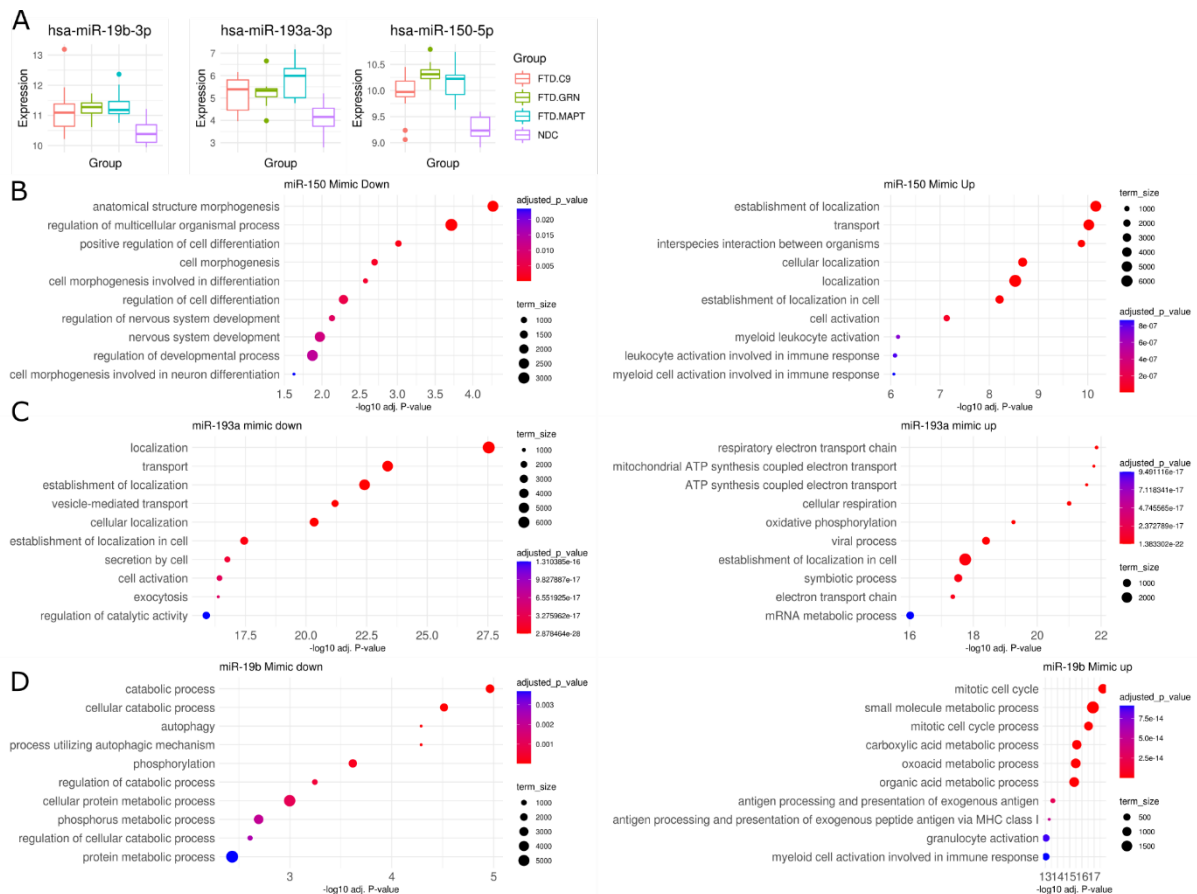


Figure 6: Effects of miRNA mimic and inhibitor experiments in iPSC-derived microglia. **A** Boxplots of normalized expression values for the selected miRNAs. **B**, **C**, **D** The top ten most significantly enriched biological processes of up- and down-regulated genes after transfection with mimics for miR-150-5p, miR-193a-3p and miR-19b-3p, respectively. Node size corresponds to the number of genes in the biological process term and node colour corresponds to the P-value adjusted for multiple testing.

Discussion

Here, we present the data from phase 1 of the RiMod-FTD project, a multi-omics, multi-model data resource for FTD research that aims to understand the role of distinct genetic risk factors in the disease. Generated by the RiMod-FTD consortium over several years, the resource depicts a valuable tool for FTD researchers that will help to accelerate scientific progress towards a better understanding of relevant disease mechanisms in FTD. Additional multi-omics data from iPSC derived cell types, transgenic mouse models and other brain regions will be added over time.

By studying post-mortem tissue of the GFM we detected largest transcriptional dysregulation and greatest neuronal loss in FTD caused by mutations in GRN, agreeing with previous findings of a more pronounced frontal lobe atrophy in FTD-GRN compared to other subtypes³². Our deconvolution analysis furthermore indicates that excitatory neurons are the most affected cell type in all genetic disease groups of FTD, which was confirmed in the RiMod-FTD proteomics data (Mediema et al., manuscript in preparation) as well. Recently, evidence from multiple studies has accumulated pointing toward a strong involvement of glutamatergic synapses in FTD³³. While it has been previously reported that densities of both ionotropic glutamate receptors, AMPA and NMDA receptors, are reduced in post-mortem brain tissue of FTD patients²¹, we see evidence that AMPA receptors are particularly affected. Intriguingly, a recent single-nucleus RNA-seq study in a GRN mouse model could show that hyperactivation of microglia leads to selective loss of excitatory neurons³⁴, which confirms our hypothesis that excitatory neurons are especially vulnerable in FTD. Strong neuroinflammation is a distinct feature of FTD-GRN, which is confirmed in our data and by increased microglial cell numbers in this FTD sub-type, in line with recent findings showing increased microglial burden in FTD-GRN^{35,36}. Using an integrative approach, we could highlight the TFs: NFKB2, RELA, KLF3 and SP1 as potential key inflammatory drivers, leading to activation of the NFkB- and TNF-signalling pathways. We have furthermore found indicators of activated necroptosis, suggesting this pathway as potential cause for cell death. The necroptosis cell death pathway is deregulated in several neurodegenerative disorders³⁷, and a recent study has shown that TBK1, a genetic cause of ALS and FTD (here down-regulated in FTD-GRN), is an endogenous inhibitor of RIPK1, an upstream regulator of RIPK3³⁸. The authors showed that embryonic lethality of TBK1-knockout mice is dependent on RIPK1 activity, suggesting that the necroptosis pathway is indeed an important part of FTD pathogenesis. In a recent review, Molnár and colleagues have discussed several available drugs that could potentially regulate necroptosis³⁹, highlighting the potential of this pathway as a drug target for developing therapies for FTD.

Our pathway enrichment and deconvolution analyses pointed toward increased blood vessel abundance and growth in FTD brains compared to controls, which is consistent with the results from the RiMod-FTD proteomics data (Mediema et al., manuscript in preparation). It is generally not known how and if the vasculature system is involved in FTD pathogenesis, although recent studies have observed abnormalities in a mouse model of tau pathology and post-mortem human brains^{22,23}. To our knowledge, angiogenesis as a pathological feature in

several genetic FTD subtypes has not been reported before and therefore depicts an important subject to study for future FTD research.

In all three disease groups, we have observed prominent up-regulation of ECM pathways and MMP enzymes, suggesting MMPs as important regulators in FTD pathogenesis. While it has been increasingly recognized that MMPs are important regulators in many neurodegenerative diseases^{40,41}, the role of MMPs in FTD pathogenesis has not been investigated in depth. In mouse models of ALS, inhibition of the MMPs MMP2 and MMP9 could indeed prolong survival and reduce symptoms^{42,43}. Moreover, TIMP3, which is up-regulated in our data, was found to be partly responsible for neuronal apoptosis in an ALS model⁴⁴, which points towards TIMP3 as a potential apoptosis mechanism in FTD. MMPs are furthermore tightly involved in the inflammatory response, and can activate the tumour necrosis factor (TNF) gene, for instance⁴⁵. Inflammatory cytokines, hypoxia and reactive oxygen species can lead to the activation of MMPs^{40,46}. MMPs can digest the ECM, stimulate increased production of growth factors and thereby promote the growth of blood vessels, providing a potential causal link to the prominent enrichment of endothelial cells⁴⁶. Given their important biological functions and their involvement in all genetic FTD subgroups, we think it will be fruitful and important to further investigate how MMPs contribute to FTD and whether they can be exploited as drug targets, as MMP inhibition in model system has shown promising results^{47,48}.

Impaired cellular trafficking mechanisms is very likely a key feature of FTD pathogenesis and it has been shown multiple times that FTD-causal mutations lead to trafficking deficits⁴⁹⁻⁵¹. However, it is not always clear which mechanisms continue to dysfunctional transport mechanisms. Here, using multi-omics data and validation experiments, we show that elevated expression of several miRNAs contributes to the inhibition of genes important for cellular transport. Additional studies are necessary to further validate this hypothesis, which directly suggests several miRNAs as putative drug targets.

A limitation of our study is the number of samples per group. We believe that increasing the sample size for individual groups such as FTD-C9orf72 will further increase the power of our analysis and help to better define which pathways are truly distinct to certain subtypes. It will therefore be an objective for future iterations of the RiMod-FTD resource to include larger numbers of samples.

To conclude, we present here an integrated multi-omics analysis on data from Phase 1 of the RiMod-FTD project and developed new hypotheses on FTD disease mechanisms. The data presented here highlights several regulator molecules important for FTD pathogenesis and their consequences such as vascular abnormalities and thereby we show the value of an integrated multi-omics data analysis for hypothesis generation and testing. The data from the RiMod-FTD project will be of great value to other scientists and ongoing extensions of this resource will further increase its value.

Methods

Donor samples employed in this study

Post mortem human brains

Tissues were obtained under a Material Transfer Agreement from the Netherlands Brain Bank, and additional samples were provided by the Queen Square Brain Bank of Neurological Disorders and MRC, King College London. Demographic details about human brain samples are summarized in Table S1.

GFM and GTM tissue from each subject was divided into three pieces for transcriptomic, proteomic and epigenetic experiments in a dry-ice bath using precooled scalpels and plasticware.

hiPS-derived NGN2 neurons and miRNA mimics and inhibitors transfection

smNPC were derived from hiPSc cells (Cell line id: GM23280 obtained from the Coriell Institute) using the protocol described by Reinhardt et al.⁵². The differentiation protocol from smNPC to neurons involves over-expression of Neurogenin-2 (NGN2) using a modified version of the NGN2 lentiviral inducible vector system (single vector pLV_TRET_hNgn2_UBC_BSD_T2A_rtTA3). The detailed description about protocol, reagents and media composition is available in Dhingra et al.⁵³.

Briefly, stable NGN2 smNPC are grown for six days in expansion medium N2B27 supplemented with CHIR99021 (CHIR) 3 μ M, Purmorphamine (PMA) 0.5 μ M and L-ascorbic acid 2-phosphate magnesium (AA) 64 mg/l. For differentiation, cells are plated (80,000 cells/cm²) onto Poly L-orithine and laminin coated plates in N2B27 medium supplemented with doxycycline (dox) at 2.5 μ g/mL, and 2 μ M DAPT. On day 4 of differentiation, transfection was performed in n=3 replicate plates using lipofectamine RNAiMax (ThermoFisher Scientific) with a final concentration of miRNA mimic and inhibitors (miR-19b-3p and miR-1505p mimics and inhibitors from Qiagen and miR-193a-3p mimic and inhibitor from ThermoFisher Scientific) in the range of 5 to 10 nM as per the manufactures' guidelines along with their corresponding controls. Next day (day 5 of differentiation), the complete media was changed with N2B27 media supplemented with dox, 10 ng/mL brain-derived neurotrophic factor (BDNF), 10 ng/mL glial cell-derived neurotrophic factor (GDNF), 10 ng/mL neurotrophic factor 3 (NT-3), 1 μ g/mL Laminin, and 10 μ M DAPT. Thereafter, half media was changed on day 8 of differentiation. On day 11, cells were gently washed with PBS and processed for RNA isolation.

hiPS-derived microglia and miRNA mimics and inhibitors transfection

hiPSCs were differentiated as previously described (van Wilgenburg et al.⁵⁴). In brief, 3 x 10⁶ iPSCs were seeded into an Aggrewell 800 well (STEMCELL Technologies) to form embryoid bodies (EBs), in mTeSR1 and fed daily with medium plus 50ng/ml BMP4 (Miltenyi Biotec), 50ng/ml VEGF (Miltenyi Biotec), and 20ng/ml SCF (R&D Systems). Four-day EBs were then differentiated in 6-well plates (15 EBs/well) in X-VIVO15 (Lonza) supplemented with 100ng/ml M-CSF (Miltenyi Biotec), 25ng/ml IL-3 (Miltenyi Biotec), 2mM Glutamax (Invitrogen Life Technologies), and 0.055mM beta-mercaptoethanol (Thermo Fisher Scientific), with fresh medium added weekly. Microglial precursors emerging in the supernatant after approximately 1 month were collected and isolated through a 40 μ m cell strainer and plated in N2B27 media supplemented with 100 ng/ml M-CSF, 25 ng/ml interleukin 34 (IL-34) for differentiation. Thereafter, the media is reshred every 2 days supplemented with 100 ng/ml M-CSF, and 25 ng/ml IL-34. The cells were cultured for

additional 6 days with media refresh every 2 days. On day 7 of maturation, transfection was performed in n=3 replicate plates using lipofectamine RNAiMax with a final concentration of miRNA mimics and inhibitors in the range of 5 to 10 nM as per the manufactures' guidelines along with their corresponding controls (miR-19b-3p and miR-1505p mimics and inhibitors from Qiagen and miR-193a-3p mimic and inhibitor from ThermoFisher Scientific). Next day complete media was refreshed. On day 11, cells were gently washed with PBS and processed for RNA isolation.

Genetic analysis

Genomic DNA was isolated from 50 mg of GFM frozen brain tissue by using the Qiamp DNA mini kit (Qiagen) following the manufacturer protocol. DNA concentration and purity were assessed by nanodrop measurement. DNA integrity was evaluated by loading 100 nanogram per sample on a 0,8% agarose gel and comparing size distribution to a size standard.

Presence of C9orf72-HRE in postmortem brain tissues and hIPS cells was confirmed by primed repeat PCR according to established protocols. Reported mutations for MAPT and GRN were verified by sanger sequencing.

Transcriptomic procedures

RNA isolation from human brain tissue

Total RNA for CAGE-seq and RNAseq was isolated from ± 100 mg of frozen brain tissue with TRIzol reagent (Thermo Fischer Scientific) according to the manufacturer recommendation, followed by purification with the RNeasy mini columns (Qiagen) after DNase treatment.

Total RNA for smallRNA-seq was isolated from frozen tissue using the TRIzol reagent (ThermoFischer Scientific). After isopropanol precipitation and 80% ethanol rinsing RNA pellet was resuspended in RNase free water and up to 10 micrograms of RNA was incubated with 2U of Ambion DNase I (ThermoFischer) at 37°C for 20 minutes. DNA-free RNA samples were then further purified by phenol-chloroform-isoamyl-alcohol extraction followed by ethanol precipitation.

RNA isolation from smNPC-derived neurons and microglia

Total RNA was isolated from NGN2 driven neurons and microglia cells after transfection with miRNA mimics and inhibitors. Briefly at day 11 of transfection cells were carefully rinsed with PBS and lysed in Qiazol buffer (Qiagen). Further DNase treatment and purification were carried out with the miRNeasy micro kit (Qiagen) according to the manufacturer protocol.

RNA QC

For each RNA sample, RNA concentration (A_{260}) and purity ($A_{260/280}$ and $A_{260/230}$) were determined by Nanodrop measurement and RNA integrity (RIN) was assessed on a Bioanalyser 2100 system and/or Tape station 41200 (Agilent Technologies Inc.)

CAGE-seq libraries

CAGE-seq libraries were prepared from 5 micrograms of RNA from frozen brain tissues according to a published protocol⁵⁵. Libraries were sequenced on a HiSeq 2000 and/or HiSeq2500 on a 1x50 bp single read (SR) flow cell (Illumina) at an average of 20M reads/sample.

RNAseq libraries

Total RNAseq libraries were prepared from 1 microgram of total RNA from frozen brain tissue using the TruSeq Stranded Total RNA with Ribo-Zero Gold kit (Illumina) according to the protocol specifications. RNAseq libraries were sequenced on a HiSeq2500 and HiSeq4000 on a 2x100 bp paired end (PE) flow cell (Illumina) at an average of 100M PE/sample.

smallRNAseq libraries

Small RNA-seq libraries were prepared from 1 microgram of total RNA from NPC-derived neurons and 300 nanograms of microglia after miRNA mimics and inhibitors transfection, using the mRNA TrueSeq Stranded kit (Illumina). mRNAseq libraries were sequenced on a NextGen550 on a 75 cycles flow cell (Illumina). Small RNAseq libraries from frozen tissue were prepared starting from 2 micrograms of total RNA using the Nextflex Small RNA-seq kit v3 (Bioo Scientific) and the NEBNext Small RNA library prep set for Illumina (New England Biolabs). Libraries were sequenced on a NextSeq550 on a 75 cycles flow cell.

Methylation assay

To assess the methylation status of over 850000 CpG sites in promoter, gene body and enhancer regions we have used the MethylationEPIC bead chip arrays (Illumina). Bisulfite conversion of genomic DNA, genome amplification, hybridization to the beadchips, washing, staining and scanning procedure was performed by Atlas Biolabs (Atlas Biolabs, Berlin, Germany). Cases and controls DNAs were distributed randomly across each array.

HumanBase Module Analysis

Functional gene modules were generated using the HumanBase tool at: <https://hb.flatironinstitute.org/>. We divided DEGs into up- and down-regulated genes as we were looking for active and repressed modules in FTD. Modules were downloaded for further analysis. Cell type enrichment analysis was performed for genes of each modules using EWCE⁵⁶ as described further down.

RNA-seq processing and analysis

Raw FastQ files were processed using the RNA-seq pipeline from nf-core (nf-core/rnaseq v1.3)⁵⁷, with trimming enabled. Gene quantification was subsequently done using Salmon (v0.14.1)⁵⁸ on the trimmed FastQ files. Alignment and mapping were performed against the human genome hg38. DESeq2 (v.1.26.0)⁵⁹ was used to perform differential expression analysis. We corrected for the covariates gender and PH-value. Genes were considered differentially expressed when having a Benjamini-Hochberg corrected P-value below 0.05.

Cell type deconvolution and filtering

We performed cell type deconvolution on the RNA-seq data using Scaden⁶⁰. For training we used the human brain training dataset used in the Scaden publication. Each ensembl model was trained for 5000 steps. To filter differentially expressed genes for false positives caused by cell composition bias, we first calculated the correlation of gene expression with cell type fraction. Then, we calculated a cell type specificity score as defined in Skene et al.⁵⁶ for each gene available in the scRNA-seq dataset from Darmanis et al.⁶¹. We filtered out all genes that had a specificity score of at least 0.5 and a positive correlation of at least 0.4 with the cell type fractions of the most specific cell type. False positive DEGs that are caused by

systematic increase or decrease of a specific cell type will show high correlation with the cell type fractions and can thus be identified and removed from the analysis. A specificity score of 0.5 means that half of the total gene expression for a certain gene can be attributed to a single cell type, assuming a uniform cell type composition. The cut-offs for specificity score and correlation were chosen based on an informed decision. Relative changes in cell type composition were quantified by first calculating the average fractions of a cell type for all groups and then calculating the percentual change of cell fractions compared to the average control fractions. This allows to detect relative changes in cell type compositions. Statistical significance between cell type fractions of groups was assessed using a t-test in the R language.

Cell type enrichment analysis

We performed cell type enrichment analysis of genesets using the EWCE R package⁵⁶. Cell type specificity of genes was calculated from the single-cell RNA-seq cortex dataset of Darmanis and colleagues⁶¹. EWCE analysis was done following instructions from <https://github.com/NathanSkene/EWCE>.

CAGE-seq processing and analysis

Sequencing adapters and barcodes in CAGE-seq FastQ files were trimmed using Skewer (v.0.1.126)⁶². Sequencing artefacts were removed using TagDust (v1.0)⁶³. Processed reads were then aligned against the human genome hg38 using STAR (v.2.4.1)⁶⁴. CAGE detected TSS (CTSS) files were created using CAGER (v1.10.0)⁶⁵. With CAGER, we removed the first G nucleotide if it was a mismatch. CTSS were clustered using the 'distclu' method with a maximum distance of 20 bp. For exact commands used we refer to the reader to the scripts used in this pipeline: <https://github.com/dznetubingen/cageseq-pipeline-mf>.

Transcription factor activity analysis

To identify candidate regulatory transcription factors, we first performed differential expression analysis with all CAGE-seq clusters (see RNA-seq analysis). Then, we extracted the sequence 600 bp up-stream and 300 bp downstream around all detected clusters. We used Homer⁶⁶ to look for significant TFBS enrichment in the regions around up- and down-regulated clusters (similar to⁶⁷). TFBS motifs were downloaded from the JASPAR database⁶⁸. When calculating enrichment, we considered all extracted regions that are not part of the set of interest as background. The complete pipeline can be found at <https://github.com/KevinMenden/tf-activity>. We selected all TFs with significant enrichment (p-value ≤ 0.001) for either up-regulated or down-regulated CAGE clusters as candidate regulators. We considered genes as potential targets of a TF if a TFBS could be found in their promoter region. As an additional filter, we selected only TFs with evidence for differential expression in the RNA-seq data (adj. P-value < 0.05 , not filtered for cell composition).

smRNA-seq processing and analysis

After removing sequencing adapters, all FastQ files were uploaded to OASIS2⁶⁹ for analysis. Subsequent differential expression analysis was performed on the counts yielded from OASIS2, using DESeq2 and correcting for gender and PH-value, as was done for the RNA-seq data. Additionally, we added a batch variable to the design matrix to correct for the two different batches of this dataset. For the target prediction analysis, we first downloaded all targets from mirBase⁷⁰. Then, we correlated the expression of miRNAs with their

predicted targets using matching samples from the RNA-seq data. We removed all predicted targets with a correlation above -0.4, thus only considering miRNA-target pairings with high negative correlation.

Methylation data processing and analysis

The Infinium MethylationEPIC BeadChip data was analyzed using the minfi R package⁷¹. We removed all sites with a detection P-value above 0.01, on sex chromosomes and with single nucleotide polymorphisms (SNPs). Data normalization was done using stratified quantile normalization. Sites with a standard deviation below 0.1 were considered uninformative and filtered out, to increase detection power. Surrogate variable analysis⁷² was performed to determine confounding factors. Differential methylation analysis was done using the limma package⁷³ and controlling for the detected surrogate variables. Sites with a Benjamini-Hochberg⁷⁴ adjusted P-value below 0.05 were considered differentially methylated.

Age prediction

We predicted the biological age of donors using the methylation data and the Wenda algorithm⁷⁵. Training data was kindly provided by the authors of Wenda. We subsetted the data for CpG sites found in our data (11,729) sites and performed the prediction as described at <https://github.com/PfeiferLabTue/wenda>.

Analysis of mRNA-seq data from cellular models

This section describes the analysis of mRNA-seq data generated for the miRNA mimic and inhibitor experiments. FastQ files were mapped and gene counts quantified using Salmon and differential expression analysis was performed with DESeq2 (see post-mortem brain RNA-seq analysis). DEGs were examined for pathway enrichment using go:Profiler.

Assessment of degeneration

For assessment of neurodegeneration, H&E stained paraffin sections of the frontal and temporal cortex were graded as absent (0), mild (1), moderate (2) and severe (3) based on the presence of spongiosis, neuronal loss and gliosis.

Data Availability

All data used in this study and published as phase 1 of the RiMod-FTD resource will be deposited at the European Phenome-genome Archive (EGA) upon publication.

Code Availability

The code used for generating the analysis results is made freely available in the GitHub repository <https://github.com/dznetubingen/rimod-ftd-paper>.

References

1. Bang, J., Spina, S. & Miller, B. L. Frontotemporal dementia. *Lancet* **386**, 1672–1682 (2015).
2. Panza, F. *et al.* Development of disease-modifying drugs for frontotemporal dementia

- spectrum disorders. *Nat. Rev. Neurol.* **16**, 213–228 (2020).
3. Seelaar, H., Rohrer, J. D., Pijnenburg, Y. A. L., Fox, N. C. & van Swieten, J. C. Clinical, genetic and pathological heterogeneity of frontotemporal dementia: a review. *J. Neurol. Neurosurg. Psychiatry* **82**, 476–486 (2011).
 4. Olszewska, D. A., Lonergan, R., Fallon, E. M. & Lynch, T. Genetics of Frontotemporal Dementia. *Current Neurology and Neuroscience Reports* vol. 16 (2016).
 5. Sirkis, D. W., Geier, E. G., Bonham, L. W., Karch, C. M. & Yokoyama, J. S. Recent Advances in the Genetics of Frontotemporal Dementia. *Curr. Genet. Med. Rep.* **7**, 41–52 (2019).
 6. Sieben, A. *et al.* The genetics and neuropathology of frontotemporal lobar degeneration. *Acta Neuropathologica* vol. 124 353–372 (2012).
 7. Balendra, R. & Isaacs, A. M. C9orf72-mediated ALS and FTD: multiple pathways to disease. *Nat. Rev. Neurol.* **1** (2018) doi:10.1038/s41582-018-0047-2.
 8. RiMod-FTD | JPND. <https://www.neurodegenerationresearch.eu/initiatives/annual-calls-for-proposals/closed-calls/risk-factors-2012/risk-factor-call-results/rimod-ftd/>.
 9. Raudvere, U. *et al.* g:Profiler: a web server for functional enrichment analysis and conversions of gene lists (2019 update). *Nucleic Acids Res.* **47**, W191–W198 (2019).
 10. Golpich, M. *et al.* Mitochondrial Dysfunction and Biogenesis in Neurodegenerative diseases: Pathogenesis and Treatment. *CNS Neurosci. Ther.* **23**, 5–22 (2017).
 11. Li, Y., Li, Z.-X., Jin, T., Wang, Z.-Y. & Zhao, P. Tau Pathology Promotes the Reorganization of the Extracellular Matrix and Inhibits the Formation of Perineuronal Nets by Regulating the Expression and the Distribution of Hyaluronic Acid Synthases. *J. Alzheimer's Dis.* **57**, 395–409 (2017).
 12. Végh, M. J. *et al.* Reducing hippocampal extracellular matrix reverses early memory deficits in a mouse model of Alzheimer's disease. *Acta Neuropathol. Commun.* **2**, (2014).
 13. Lu, P., Takai, K., Weaver, V. M. & Werb, Z. Extracellular Matrix degradation and remodeling in development and disease. *Cold Spring Harb. Perspect. Biol.* **3**, (2011).
 14. Duits, F. H. *et al.* Matrix Metalloproteinases in Alzheimer's Disease and Concurrent Cerebral Microbleeds. *J. Alzheimer's Dis.* **48**, 711–720 (2015).
 15. Xi, Z. *et al.* Hypermethylation of the CpG Island Near the G 4 C 2 Repeat in ALS with a C9orf72 Expansion. *Am J Hum Genet* 981–989 (2013) doi:10.1016/j.ajhg.2013.04.017.
 16. Biswas, M. H. U. *et al.* MMP-9 and MMP-2 Contribute to Neuronal Cell Death in iPSC Models of Frontotemporal Dementia with MAPT Mutations. *Stem Cell Reports* **7**, 316–324 (2016).
 17. Young, J. J., Lavakumar, M., Tampi, D., Balachandran, S. & Tampi, R. R. Frontotemporal dementia: latest evidence and clinical implications. *Ther. Adv. Psychopharmacol.* **8**, 33–48 (2018).
 18. Cash, D. M. *et al.* Patterns of gray matter atrophy in genetic frontotemporal dementia: results from the GENFI study. *Neurobiol. Aging* **62**, 191–196 (2018).
 19. Fu, H., Hardy, J. & Duff, K. E. Selective vulnerability in neurodegenerative diseases. *Nat. Neurosci.* **21**, 1350–1358 (2018).
 20. Paiese, F. *et al.* Anti-GluA3 antibodies in frontotemporal dementia: effects on glutamatergic neurotransmission and synaptic failure. *Neurobiol. Aging* **86**, 143–155 (2020).
 21. Murley, A. G. & Rowe, J. B. Neurotransmitter deficits from fronto temporal lobar degeneration. *Brain* **141**, 1263–1285 (2018).
 22. Bennett, R. E. *et al.* Tau induces blood vessel abnormalities and angiogenesis-related gene expression in P301L transgenic mice and human Alzheimer's disease. *Proc. Natl. Acad. Sci. U. S. A.* **115**, E1289–E1298 (2018).
 23. Ek Olofsson, H. & Englund, E. A cortical microvascular structure in vascular dementia, Alzheimer's disease, frontotemporal lobar degeneration and nondemented controls: a sign of angiogenesis due to brain ischaemia? *Neuropathol. Appl. Neurobiol.* **45**, 557–569 (2019).

24. Park, L. *et al.* Tau induces PSD95–neuronal NOS uncoupling and neurovascular dysfunction independent of neurodegeneration. *Nat. Neurosci.* **23**, 1079–1089 (2020).
25. Greene, C. S. *et al.* Understanding multicellular function and disease with human tissue-specific networks. *Nat. Genet.* **47**, 569–576 (2015).
26. Skene, N. G. & Grant, S. G. N. Identification of Vulnerable Cell Types in Major Brain Disorders Using Single Cell Transcriptomes and Expression Weighted Cell Type Enrichment. *Front. Neurosci.* **10**, 16 (2016).
27. Paushter, D. H., Du, H., Feng, T. & Hu, F. The lysosomal function of progranulin, a guardian against neurodegeneration. *Acta Neuropathol.* **136**, 1 (2018).
28. Lui, H. *et al.* Progranulin Deficiency Promotes Circuit-Specific Synaptic Pruning by Microglia via Complement Activation. *Cell* **165**, 921–935 (2016).
29. Krabbe, G. *et al.* Microglial NFκB-TNFα hyperactivation induces obsessive-compulsive behavior in mouse models of progranulin-deficient Frontotemporal dementia. *Proc. Natl. Acad. Sci. U. S. A.* **114**, 5029–5034 (2017).
30. Martens, L. H. *et al.* Progranulin deficiency promotes neuroinflammation and neuron loss following toxin-induced injury. *J. Clin. Invest.* **122**, 3955–3959 (2012).
31. Zou, M. *et al.* Autophagy inhibition of hsa-miR-19a-3p/19b-3p by targeting TGF-β R II during TGF-β1-induced fibrogenesis in human cardiac fibroblasts. *Sci. Rep.* **6**, 1–15 (2016).
32. Whitwell, J. L. *et al.* Neuroimaging signatures of frontotemporal dementia genetics: C9ORF72, tau, progranulin and sporadics. *Brain* **135**, 794–806 (2012).
33. Benussi, A. *et al.* Toward a glutamate hypothesis of frontotemporal dementia. *Front. Neurosci.* **13**, (2019).
34. Zhang, J. *et al.* Neurotoxic microglia promote TDP-43 proteinopathy in progranulin deficiency. *Nature* (2020) doi:10.1038/s41586-020-2709-7.
35. Woollacott, I. O. C. & Rohrer, J. D. The clinical spectrum of sporadic and familial forms of frontotemporal dementia. *J. Neurochem.* **138**, 6–31 (2016).
36. Sakae, N. *et al.* Microglia in frontotemporal lobar degeneration with progranulin or C9ORF72 mutations. *Ann. Clin. Transl. Neurol.* **6**, 1782–1796 (2019).
37. Yuan, J., Amin, P. & Ofengeim, D. Necroptosis and RIPK1-mediated neuroinflammation in CNS diseases. *Nat. Rev. Neurosci.* **20**, 19–33 (2019).
38. Xu, D. *et al.* TBK1 Suppresses RIPK1-Driven Apoptosis and Inflammation during Development and in Aging. *Cell* **174**, 1477-1491.e19 (2018).
39. Molnár, T. *et al.* Current translational potential and underlying molecular mechanisms of necroptosis. *Cell Death Dis.* **10**, 1–21 (2019).
40. Brkic, M., Balusu, S., Libert, C. & Vandenbroucke, R. E. Friends or Foes: Matrix Metalloproteinases and Their Multifaceted Roles in Neurodegenerative Diseases. *Mediators Inflamm.* **2015**, (2015).
41. Rivera, S., García-González, L., Khrestchatsky, M. & Baranger, K. Metalloproteinases and their tissue inhibitors in Alzheimer’s disease and other neurodegenerative disorders. *Cell. Mol. Life Sci.* **76**, 3167–3191 (2019).
42. Kiaei, M. *et al.* Matrix metalloproteinase-9 regulates TNF-α and FasL expression in neuronal, glial cells and its absence extends life in a transgenic mouse model of amyotrophic lateral sclerosis. *Exp. Neurol.* **205**, 74–81 (2007).
43. Lorenzl, S. *et al.* The matrix metalloproteinases inhibitor Ro 26-2853 extends survival in transgenic ALS mice. *Exp. Neurol.* **200**, 166–171 (2006).
44. Lee, J. K. *et al.* Tissue inhibitor of metalloproteinases-3 (TIMP-3) expression is increased during serum deprivation-induced neuronal apoptosis in vitro and in the G93A mouse model of amyotrophic lateral sclerosis: A potential modulator of Fas-mediated apoptosis. *Neurobiol. Dis.* **30**, 174–185 (2008).
45. Vandenbroucke, R. E. *et al.* Matrix metalloproteinase 13 modulates intestinal epithelial barrier integrity in inflammatory diseases by activating TNF. *EMBO Mol. Med.* **5**, 1000–1016 (2013).
46. Rempe, R. G., Hartz, A. M. S. & Bauer, B. Matrix metalloproteinases in the brain and blood-brain barrier: Versatile breakers and makers. *J. Cereb. Blood Flow Metab.* **36**,

- 1481–1507 (2016).
47. Woo, M. S., Park, J. S., Choi, I. Y., Kimf, W. K. & Kim, H. S. Inhibition of MMP-3 or -9 suppresses lipopolysaccharide-induced expression of proinflammatory cytokines and iNOS in microglia. *J. Neurochem.* **106**, 770–780 (2008).
 48. Garcia-Alloza, M. *et al.* Matrix metalloproteinase inhibition reduces oxidative stress associated with cerebral amyloid angiopathy in vivo in transgenic mice. *J. Neurochem.* **109**, 1636–1647 (2009).
 49. Aoki, Y. *et al.* C9orf72 and RAB7L1 regulate vesicle trafficking in amyotrophic lateral sclerosis and frontotemporal dementia. *Brain* 887–897 (2017) doi:10.1093/brain/awx024.
 50. Yarwood, R., Hellicar, J., Woodman, P. G. & Lowe, M. Membrane trafficking in health and disease. *DMM Dis. Model. Mech.* **13**, (2020).
 51. Wren, M. C. *et al.* Frontotemporal dementia-associated N279K tau mutant disrupts subcellular vesicle trafficking and induces cellular stress in iPSC-derived neural stem cells. *Mol. Neurodegener.* **10**, 46 (2015).
 52. Reinhardt, P., Glatza, M., Hemmer, K., Tsytsyura, Y. & Thiel, C. S. Derivation and Expansion Using Only Small Molecules of Human Neural Progenitors for Neurodegenerative Disease Modeling. *PLoS One* **8**, 59252 (2013).
 53. Dhingra, A. *et al.* Automated production of human induced pluripotent stem cell-derived cortical and dopaminergic neurons with integrated live-cell monitoring. *J. Vis. Exp.* **2020**, 1–29 (2020).
 54. van Wilgenburg, B., Browne, C., Vowles, J. & Cowley, S. A. Efficient, Long Term Production of Monocyte-Derived Macrophages from Human Pluripotent Stem Cells under Partly-Defined and Fully-Defined Conditions. *PLoS One* **8**, (2013).
 55. Takahashi, H., Lassmann, T., Murata, M. & Carninci, P. 5' end-centered expression profiling using cap-analysis gene expression and next-generation sequencing. *Nat. Protoc.* **7**, 542–561 (2012).
 56. Skene, N. G. & Grant, S. G. N. Identification of Vulnerable Cell Types in Major Brain Disorders Using Single Cell Transcriptomes and Expression Weighted Cell Type Enrichment. *Front. Neurosci.* **10**, 16 (2016).
 57. Ewels, P., Magnusson, M., Lundin, S. & Källner, M. MultiQC: Summarize analysis results for multiple tools and samples in a single report. *Bioinformatics* **32**, 3047–3048 (2016).
 58. Patro, R., Duggal, G., Love, M. I., Irizarry, R. A. & Kingsford, C. Salmon provides fast and bias-aware quantification of transcript expression. *Nat. Publ. Gr.* **14**, (2017).
 59. Love, M. I., Huber, W. & Anders, S. Moderated estimation of fold change and dispersion for RNA-seq data with DESeq2. *Genome Biol.* **15**, (2014).
 60. Menden, K. *et al.* Deep learning-based cell composition analysis from tissue expression profiles. *Sci. Adv.* **6**, eaba2619 (2020).
 61. Darmanis, S. *et al.* A survey of human brain transcriptome diversity at the single cell level. *Proc. Natl. Acad. Sci. U. S. A.* **112**, 7285–7290 (2015).
 62. Jiang, H., Lei, R., Ding, S. W. & Zhu, S. Skewer: A fast and accurate adapter trimmer for next-generation sequencing paired-end reads. *BMC Bioinformatics* **15**, 182 (2014).
 63. Lassmann, T. TagDust2: A generic method to extract reads from sequencing data. *BMC Bioinformatics* **16**, 24 (2015).
 64. Dobin, A. & Gingeras, T. R. Mapping RNA-seq Reads with STAR. in *Current Protocols in Bioinformatics* (2015). doi:10.1002/0471250953.bi1114s51.
 65. Haberle, V., Forrest, A. R. R., Hayashizaki, Y., Carninci, P. & Lenhard, B. CAGEr: Precise TSS data retrieval and high-resolution promoterome mining for integrative analyses. *Nucleic Acids Res.* **43**, e51–e51 (2015).
 66. Heinz, S. *et al.* Simple Combinations of Lineage-Determining Transcription Factors Prime cis-Regulatory Elements Required for Macrophage and B Cell Identities. *Mol. Cell* **38**, 576–589 (2010).
 67. Arenillas, D. J. *et al.* CAGED-oPOSSUM: motif enrichment analysis from CAGE-derived TSSs. *Bioinformatics* **32**, 2858–60 (2016).

68. Khan, A. *et al.* JASPAR 2018: update of the open-access database of transcription factor binding profiles and its web framework. *Nucleic Acids Res.* **46**, D260–D266 (2018).
69. Rahman, R. U. *et al.* Oasis 2: Improved online analysis of small RNA-seq data. *BMC Bioinformatics* **19**, 54 (2018).
70. Kozomara, A., Birgaoanu, M. & Griffiths-Jones, S. MiRBase: From microRNA sequences to function. *Nucleic Acids Res.* **47**, D155–D162 (2019).
71. Aryee, M. J. *et al.* Minfi: A flexible and comprehensive Bioconductor package for the analysis of Infinium DNA methylation microarrays. *Bioinformatics* **30**, 1363–1369 (2014).
72. Leek, J. T. & Storey, J. D. Capturing Heterogeneity in Gene Expression Studies by Surrogate Variable Analysis. *PLoS Genet.* **3**, e161 (2007).
73. Ritchie, M. E. *et al.* limma powers differential expression analyses for RNA-sequencing and microarray studies. *Nucleic Acids Res.* (2015) doi:10.1093/nar/gkv007.
74. Benjamini, Y. & Hochberg, Y. Controlling the False Discovery Rate: A Practical and Powerful Approach to Multiple Testing. *J. R. Stat. Soc.* (1995).
75. Handl, L., Jalali, A., Scherer, M., Eggeling, R. & Pfeifer, N. Weighted elastic net for unsupervised domain adaptation with application to age prediction from DNA methylation data. in *Bioinformatics* vol. 35 i154–i163 (Oxford University Press, 2019).

Affiliations

- 1 German Center for Neurodegenerative Diseases, Tübingen, Germany
- 2 National Institute on Aging, National Institutes of Health, Bethesda, MD, USA
- 3 Hertie Institute for Clinical Brain Research, Tübingen, Germany
- 4 German Center for Neurodegenerative Diseases, Göttingen, Germany
- 5 Institute of Medical Systems Biology, University Medical Center Hamburg-Eppendorf, Hamburg, Germany
- 6 Neurology Unit, Department of Clinical and Experimental Sciences, University of Brescia, Italy
- 7 University of Southern California, California, USA

Acknowledgements

Post-mortem brain tissue was obtained from the Netherlands Brain Bank, Netherlands Institute for Neuroscience, Amsterdam, and from the Queen Square Brain Bank for Neurological Disorders, UCL Institute of Neurology, London.

Contributions

The project was initiated and designed by PH. Small RNA-seq experiments were performed by AF, LK, PR and NF. RNA-seq and CAGE-seq experiments were performed by CB, PR, NF, MC. iPSC-derived neuron and microglia experiments were performed by AD and DKV.

Analysis of CAGE-seq data was done by MF, TN and KM. JSS, BA and KM analysed the RNA-seq data. KM analysed the smRNA-seq and methylation data. PH, SB, PR planned and interpreted all performed analyses. KM, PH, PR and SB wrote the manuscript.

Funding

This work was funded in part by the EU Joint Programme - Neurodegenerative Disease Research (JPND) project: Risk and Modifying factors for FTD (RiMod-FTD) and the NOMIS Foundation. DKV is in receipt of an Alexander von Humboldt Research Fellowship.

RiMod-FTD Partners

Prof. Dr. P. Heutink: Kevin Menden; Margherita Francescato; Tenzin Nyima; Cornelis Blauwendraat; Burcu Atarsu; Javier Simon Sanchez; Stefan Bonn; Patrizia Rizzu; German Center for Neurodegenerative Diseases (DZNE)-Tübingen
Otfried Müller Strasse 23
72076 Tübingen
Germany
Tel.: +49 (0)7071 9254 050
E-Mail: peter.heutink@dzne.de

Prof. Dr. J. Hardy:
Reta Lila Weston Research Laboratories, Dept. of
Molecular Neuroscience, UCL Institute of
Neurology, London WC1N 3BG, England.
Tel: +44 (0) 207 679 4297.
E-Mail: j.hardy@UCL.AC.UK

Prof. Dr. A. Brice
Research Centre of the Brain and Spine Institute
(CRicm UMR_S975), Pitié-Salpêtrière Hospital, 47
boulevard de l'Hôpital, 75013 Paris, France
Tel: +33 1 572746 82
E-Mail: alexis.brice@upmc.fr

Prof. Dr. J.C. van Swieten; Fenne Riemsdagh
Prof. Dr. A.B. Smit; Pim van Nierop; Suzanne Miedema
Dept. Neurology, ErasmusMC, 's-Gravendijkwal 230
3015 CE Rotterdam, Netherlands.
Tel: +31 107033274
E-Mail: j.c.vanswieten@erasmusmc.nl

Prof. Dr. P. Longone/
Prof. Dr. E. Buratti/
Prof. Dr. A. Alberici
Molecular Neurobiology Unit
Santa Lucia Foundation
Via del Fosso di Fiorano 64

00179 Roma Italia
Tel. +39-06501703151
E-Mail: p.longone@hsnatalucia.it

Prof. Dr. P. van Damme
Laboratory for Neurobiology (Vesalius Research
Center) O&N IV Herestraat 49 - bus 912.
3000 Leuven, Belgium
Tel. +32 16 3 73181
E-Mail: philip.vandamme@vib-kuleuven.be

Dr. A. Sandelin
Department of Biology, Copenhagen University,
Ole Maasøes vej 5,
DK2200 Copenhagen, Denmark.
Tel +45 35321285/ Email: albin@binf.ku.dk

Prof. Dr. A. Fischer
Dept. of Psychiatry and Psychotherapy, University
of Göttingen, German Center for Neurodegenerative
Diseases (DZNE) Göttingen, Grisebach Str. 5,
37077 Göttingen, Germany.
Tel: +49 551 30178.
E-Mail: afische2@gwdg.de

Prof. Dr. S. Lichtenthaler
Technical University Munich (TUM) and German
Center for Neurodegenerative Diseases (DZNE),
Max-Lebsche Platz 30, 81377 Munich, Germany.
Tel: +49 89 7095 8405
E-Mail: stefanlichtenthaler@dzne.de

Prof. Dr. E. Mandelkow + Prof. Dr. E. Mandelkow + Marta Anglada
German Center for Neurodegenerative Diseases
(DZNE), Ludwig-Erhard-Allee 2 53175 Bonn,
Germany.
Tel: +49 (0) 228 / 43302-630
E-Mail: eckhard.mandelkow@dzne.de